FINITE ELEMENT MODELING OF CRACKED BODIES

USING THE BODNER-PARTOM FLOW LAW

T. Nicholas and M. Bohun
Air Force Wright Aeronautical Laboratories
Wright Patterson Air Force Base, Ohio 45433

The Bodner-Partom flow law which models viscoplastic material behavior has been used to represent two nickel-base superalloys, Gatorized IN100 and Inconel 718 at elevated temperature. Procedures for the determination of the material parameters are presented along with a discussion of the physical significance of each parameter. The material model is then used in finite element computations to evaluate the response of cracked bodies to monotonic, sustained, or cyclic loading. Geometries investigated include the center cracked panel, the compact tension specimen, and the single cracked ring under tension. A Hybrid Experimental Numerical (HEN) procedure has been used to deduce crack growth rates from experimental displacement measurements which are input into finite element computations. The results of several studies conducted over the last several years are summarized.

INTRODUCTION

Sustained load crack growth data are often difficult to obtain at elevated temperatures for several reasons. Optical measurements of surface crack length produce large amounts of scatter when the oxidized surface reduces the visibility at high temperatures. Localized inelastic deformation in the vicinity of the crack tip makes the exact determination of surface crack length ambiguous and usually leads to variability in observations from one observer to another. Tunneling, where the interior of the specimen grows at a faster rate than on the surface, leads to erroneous crack length data when surface measurements are used. Very low crack growth rates, leading to small amounts of crack extension, can compound the difficulties associated with determining crack growth rates. For long-term tests, around the clock and weekend observations are required which are often impractical. As alternatives to optical measurements, automated data acquisition systems provide desirable features. Electric potential drop measurements, although requiring sophisticated equipment and calibration, can provide continuous data on crack length. Compliance measurements from periodic unloading and reloading can provide discrete crack length values in the absence of an observer. The simplest measurement, however, is a continuous displacement measurement across two suitably chosen points under constant load. If these displacement values can be related to crack extension, crack length data can be obtained easily and continuously.

A procedure has been developed for determining crack length from displacement measurements during sustained load crack growth tests. This procedure, labeled the Hybrid Experimental Numerical (HEN) method, utilizes experimental displacement data in finite element method computations where a realistic constitutive model describing the material behavior is incorporated. The model describes time-dependent viscoplastic flow in an incremental strain rate equation with a single state variable which includes the materials history of loading. The constants for the model are obtained from constant strain rate tests and creep data. The model has been incorporated into a constant strain triangle finite element program which is used in the HEN procedure. This procedure has been applied to several cracked specimen geometries using different displacement measurement techniques and locations. In addition, the finite element program has been used to evaluate the stress and strain states in cracked bodies under cyclic loading. This paper presents a review of these applications of the finite element method to cracked geometries.

BODNER-PARTOM FLOW LAW

The constitutive equations used to describe the elevated temperature viscoplastic material behavior in this investigation are those of Bodner and Partom.(ref. 1) The equations represent time-dependent viscoplastic flow over a wide range of strain rates using a state variable and are of the incremental type which does not require a yield surface. Total strain rate is decomposed into nonzero elastic and inelastic portions. The elastic portion is given by the time derivative of Hookes law while the inelastic portion takes the form

$$\dot{\epsilon}_{ij}^{p} = D_o \exp\left[\frac{-(n+1)}{2n}\left(\frac{Z^2}{3J_2}\right)^n\right] J_2^{-\frac{1}{2}} s_{ij} \qquad (1)$$

where D_o and n are material constants, J_2 and s_{ij} represent the second invariant and the components of the deviatoric stress tensor, respectively, and Z is a history dependent state variable representing the materials resistance to plastic flow. The evolution equation for Z is given in rate form

$$\dot{Z} = m(Z_1 - Z)W_p - AZ_1\left(\frac{Z-Z_2}{Z_1}\right)^r \qquad (2)$$

where m, Z_1, Z_2, A, and r are material constants and W_p is plastic work. In total, there are 7 constants to be determined from experimental data. A procedure has been developed by Stouffer (ref. 2) to determine the constants from constant strain rate stress-strain data and creep curves. This procedure was applied to Gatorized IN100 at 732°C. The constants used in the computations described here were obtained from that investigation. Further refinements to the procedure and a parametric study of the effects of each constant on material behavior were presented by Beaman (ref. 3) who obtained the constants for Inconel 718 at 649°C.

Determination of Constants

The constant D_o represents the limiting plastic strain rate or the rate at which applied stresses tend to infinity to sustain that strain rate. It can be chosen as 10^6/second for most metals and has been used as 10^4 in previous investigations. Unless high strain rate behavior is being evaluated, any value above the range of strain rates being computed is adequate. We recommend fixing the value at 10^6. The next pair of constants to be evaluated are n and Z_1. The strain rate sensitivity at conventional testing rates is determined by n. The value of Z_1 represents the maximum value or saturation value of Z. For the Bodner-Partom model, stress-strain curves at conventional constant strain rates asymptote towards a constant value of stress. At this stress, the material is fully saturated, ie $Z=Z_1$. At conventional strain rates, furthermore, the second term in eq. (2) can be neglected. The procedure for determining n and Z_1 is to obtain values of saturation stress for several (at least two) constant strain rate tests over several decades in strain rate. The uniaxial version of the flow law is written as

$$\dot{\varepsilon}^p = \frac{2}{\sqrt{3}} D_o \frac{\sigma}{|\sigma|} \exp\left[-\tfrac{1}{2}\left(\frac{Z}{\sigma}\right)^{2n}\left(\frac{n+1}{n}\right)\right] \qquad (3)$$

Setting $Z=Z_1$ in eq. (3) and rearranging term leads to

$$\ln\left[-\ln\frac{\sqrt{3}}{2D_o}\dot{\varepsilon}^p\right] = -2n\ln\sigma + \left[2n\ln Z_1 + \ln\left(\frac{n+1}{2n}\right)\right] \qquad (4)$$

The first term, which involves $\dot{\varepsilon}^p$, is linearly related to $\ln\sigma$. Plotting the experimental data and fitting the best straight line will provide a value -2n for the slope. From n, a value of Z_1 can be determined from eq. (3) from any pair of values of $\dot{\varepsilon}^p$ and σ along the straight line. Considering again the high strain rate regime where the recovery term in eq. (2) can be neglected, eq. (2) can be written in differential form and integrated to yield

$$\ln(Z_1 - Z) = \ln(Z_1 - Z_o) - mW_p \qquad (5)$$

where Z_o is the initial hardness when no plastic work has been expended. From a stress-strain curve at a constant (high) rate, values of Z can be computed for corresponding values of W_p allows the determination of Z_o as the extrapolated value for $W_p \to 0$ which are obtained by integrating the area under the stress-plastic strain curve. Plotting $\ln(Z_1-Z)$ against plastic work W_p allows the determination of Z_o as the extrapolated value for $W_p = 0$ from a best linear fit to the data. The slope of this line will define the value for m which controls the shape of the stress-strain curve.

If material behavior at very low strain rates, in the creep regime, is to be modeled, the second term in eq. (2) has to be used. Determination of the constants A, r, and Z_2 requires creep or very low rate stress-strain data. Note that the saturation

stress in a stress-strain test at very low constant strain rate is equivalent to an applied stress in a creep test causing a steady second stage creep rate. The constants can be determined by matching the experimental data on a plot of ln strain rate against stress as shown in Fig. 1a. For steady state values, ie constant strain rate under constant stress or vice versa, Z must achieve a steady state value from eq. (3) and, thus, $\dot{Z}$ must be zero in eq. (2). These two equations, when combined, provide a functional relation between the non-dimensional quantities $\dot{\varepsilon}^p/D_o$ and σ/Z_1. Figure 1a shows the overall behavior of the curve and the regions affected by the several constants. Figures 1b, c, and d show the effects of varying each of the constants, A r, and Z_2 individually. These curves also show the insensitivity to these constants at the higher strain rates. An interactive computer program with graphical display of the equations has been found useful in determining the constants A, r, and Z_2 by trial and error manipulation. Basically, each constant controls one aspect of the curve, ie either slope or location of an inflection point. Following the procedure outlined above in the correct order makes it relatively easy to arrive at the Bodner-Partom constants from uniaxial data.

THE HEN PROCEDURE

The hybrid experimental numerical procedure (HEN) was developed by Hinnerichs (ref. 4) to determine creep crack growth rates from expermental displacement measurements. The procedure uses a finite element computer program called VISCO (ref. 4) and utilizes the Bodner-Partom equations to describe the inelastic material behavior. These equations are incorporated into the VISCO computer code which uses constant strain triangular elements. The code computations utilize experimental displacement data as input in the HEN procedure. Essentially, the HEN procedure compares experimental displacements at a fixed point on a specimen to finite element model displacements at the same fixed experimental point. If the finite element displacement values (including creep and plasticity) are below the experimental ones, the crack is allowed to extend by popping a node. In this manner, increments of crack extension occur by node popping in the finite element scheme. Figure 1 shows a schematic of a center cracked specimen which was utilized by Hinnerichs et al (ref. 5) in the first application of the HEN procedure to determine creep crack growth rates in IN100. The experimental displacements were determined by Sharpe (ref. 6) using a laser interferometric technique which has a measurement precision of approximately 0.01 micron. The center cracked panel specimen was 25 mm wide by 7.6 mm thick. Displacements were obtained across two closely spaced microhardness indents on either side of the initial crack at distances of approximately 0.1 mm behind the crack tip as shown schematically in figure 2.

The computational scheme provides displacements at the measurement location from creep strains in the cracked specimen under sustained load. Figure 3a shows the computed displacements (NO CRACK GROWTH) compared to the experimental values. It is seen that the computed values are much less than those measured. The reason

is that the crack is extending in the experiment which increases the compliance of the specimen. To match the experimental displacement measurements, the HEN procedure provides for node popping to simulate crack growth. Nodes are popped whenever additional displacements are required to match the experimental values. In figure 3a, the points labeled RUN S2 show the displacements matched to the experimental data through the appropriate node popping. The node popping simulates the crack growth as seen in figure 3b. From the slope of the crack extension versus time plots for each of the experiments, a series of crack growth rates were obtained. These values are plotted against stress intensity factor in figure 4 and show very good correlation with creep crack growth data obtained by Donath et al (ref. 7) at higher K values. Additionally, the total amounts of crack extension computed for each numerically simulated experiment agreed very closely with those measured on the fracture surface of the specimen. In most of these cases, very small amounts of crack growth were obtained (see fig. 3b, for example).

Computational Procedure

The finite element analysis uses the residual force method to incorporate nonlinear viscoplastic material behavior into VISCO. This method increments time directly, but load, strain and stress are incremented indirectly through a time integration procedure. To implement the residual force method, the plastic strain rate of the material is determined from the Bodner-Partom constitutive eqns. (1) and (2) described in the previous section. Using the current time increment dt^i and the plastic strain rate, $\dot{\varepsilon}_{ij}^{p}$, the incremental plastic strain vector is

$$\left\{d\varepsilon_{ij}^{p}\right\}^{i} = \left\{\dot{\varepsilon}_{ij}^{p}\right\} dt^{i} \tag{6}$$

where the superscript "i" represents the current time increment. The total plastic strain is then computed from the incremental plastic strain from eqn. (6) as

$$\left\{\varepsilon_{ij}^{p}\right\}^{i} = \left\{\varepsilon_{ij}^{p}\right\}^{i-1} + \left\{d\varepsilon_{ij}^{p}\right\}^{i} \tag{7}$$

where $\left\{\varepsilon_{ij}^{p}\right\}^{i}$ is the total plastic strain at the current time increment. Next, the plastic load vector $\{Q\}$, representing the nodal forces generated by viscoplasticity is formulated as

$$\{Q\}^{i-1} = \int_{Vol} [B]^{T} [D] \left\{\varepsilon_{ij}^{p}\right\}^{i} dVol \tag{8}$$

where $[B]^T$ is the transposed strain-displacement matrix and [D] is the stress-strain matrix. The plastic load vector is then added to the current nodal loads $\{P\}^i$ to determine the current nodal displacements, computed by

$$\{U\}^{i} = [K]^{-1} \left(\{P\}^{i} + \{Q\}^{i-1}\right) \tag{9}$$

where $[K]^{-1}$, is the inverse elastic stiffness matrix and $\{U\}^i$ is the nodal displacement vector. The total strain vector is then computed by

$$\{\varepsilon_{ij}\}^i = [B]\{U\}^i \tag{10}$$

Finally, the stress is updated using eqns. (7) and (10),

$$\{\sigma_{ij}\}^i = [D]\left(\{\varepsilon_{ij}\}^i - \{\varepsilon_{ij}^p\}^i\right) \tag{11}$$

where $\{\sigma_{ij}\}^i$ is the current updated stress. This becomes the new stress value to be entered into the constitutive model to generate a new viscoplastic strain rate. This procedure continues for each time increment until the desired simulation time for the problem is reached.

Application to CT Geometry

The Hen procedure was subsequently applied to the compact tension (CT) specimen geometry (ref. 8) using experimental displacement data of Donath et al (ref. 7). Displacements were obtained off E-shaped plates fixed to the top and bottom of the specimen along the load line using LVDT's. These specimens were 5.4 mm thick and were tested using initial K values ranging from 33.0 to 49.5 $MPa\cdot m^{\frac{1}{2}}$. Figure 5a shows the finite element mesh used in these computations. Figure 5b shows displacement data for one of the specimens for the early part of the test. The crack extensions computed from these data using the HEN procedure are shown in figure 5c. The data for the entire test which involved a considerable amount of crack extension are presented in figure 5d. It can be seen that the computed values follow those labeled "effective length" fairly well. The effective lengths were obtained from unloading compliance measurements taken periodically during the sustained load test. There was fairly severe tunneling in all of the tests after the crack had extended several millimeters. The final crack lengths, as determined from the numerical computations using the HEN procedure, agreed with these from the fracture surface better than those determined from compliance measurements!

Application to a Ring Geometry

The third type of specimen was a 6 mm thick circular ring having an outside diameter of 76 mm and an inner diameter of 38 mm. The ring is loaded in tension using a pin and clevise arrangement and is cracked from the inner diameter at a location 90° from the two loading pins as shown in figure 6 which also shows the finite element mesh details. The stress intensity solution for this geometry shows a region of nearly constant K over half the thickness of the ring. Displacements were obtained across the two loading pins using LVDT's. Since load is constant and the tests are under isothermal conditions, the differential displacements are not affected by deflection of the load train or pins after the

initial load is applied. The numerical solution in the HEN procedure is, however, very sensitive to the manner in which the load is applied to the finite element grid.

The displacement measurements along with experimental data on crack length from compliance measurements were obtained by Donath et al (ref. 7). There was considerable scatter in the experimentally determined crack lengths and difficulty in correlating total crack extension with that measured on the fracture surfaces. The displacement data, on the other hand, appeared to be smoother and more consistent. For this reason, the HEN procedure was applied to obtain a somewhat independent determination of crack extension in the same specimens. Results of a typical case are presented in figure 7. Crack extension versus time from the HEN procedure are compared to the experimental data. The final crack lengths from the HEN procedure agreed closely with those obtained experimentally. In figure 8, the stress in the "y" direction is plotted versus horizontal distance ahead of the crack tip after various crack extensions. These stresses are determined at the centroid of each triangular element ahead of the crack tip which has the same dimensions, therefore, element size effects are eliminated. Notice that the peak stress at a crack length of 8.26 mm (.325 in) is 955 MPa (138.5 KSI) but drops to 782 MPa (113.4 KSI) after 3.18 mm (.125 in) of crack growth. This peak stress reduces slightly with each subsequent crack advance. As the crack advances, the stress distribution becomes sharper indicating that as the crack propagates to the edge of the ring, stresses ahead of the crack are greatly reduced as the other side of the ring carries the major load.

CRACKED BODIES UNDER CYCLIC LOADING

The Bodner-Partom constitutive equations have been used in finite element computations to determine the stress and strain fields in a compact tension specimen in the vicinity of the crack tip when the specimen is subjected to cyclic loading. The VISCO computer code was used in these investigations. In the application of the Bodner-Partom equations, no modifications were made to account for kinematic versus isotropic hardening behavior of the material. The material was assumed to undergo isotropic hardening during cyclic loading. The first problem investigated was that of a CT specimen under cyclic loading at various frequencies at a stress ratio (ratio of minimum to maximum applied load) of 0.1. The uniaxial response of the constitutive model to an applied cyclic load of load ratio 0.1 was also computed for comparison. Figure 9a shows the uniaxial response to a maximum stress of 1241 MPa at a frequency of 0.167 Hz. Figure 9b shows the effective stress versus strain in an element directly ahead of the crack tip. It was observed in both the uniaxial model and the CT specimen at the crack tip that strain continued to accumulate under cyclic loading. In the CT specimen, the element ahead of the crack tip appears to cycle under more or less fixed stress limits. The finite element computations were able to provide additional details of the stress and strain fields around the crack tip. Figure 10

shows the stress profile ahead of the crack tip after 2½ cycles and then after a 15 min hold at maximum load. It can be seen that there is a slight change in the stress field during the hold time. Experimentally, sustained load crack growth occurs at this K value of 38.5 MPa·$m^{\frac{1}{2}}$. To simulate this crack extension, a node was released. The results, shown in figure 10, indicate that the stress field with respect to the position of the crack tip has not changed. This is in contrast to the results in the ring tests where there was a change with crack extension (see fig. 8).

A similar study was carried out to evaluate the stress and strain field under fully reversed cyclic loading in a CT geometry (ref. 10). Figure 11 shows the displacement profile behind the crack tip at various load levels. It can be seen that residual displacements due to inelastic deformation have occured. At zero load, there is crack opening a small distance behind the crack tip. In these numerical exercises, no account was taken of any plastic wake which formed behind the crack due to prior cycling.

CONCLUSIONS

The Bodner-Partom flow law is a realistic representation of material behavior in nickel base superalloys at elevated temperatures. The use of this model in finite element computations of stress fields in cracked bodies provides valuable insight into elevated temperature creep and fatigue phenomenology. These tools are also very valuable in predicting sustained load crack growth rates from experimental displacement data using a hybrid-experimental-numerical procedure.

REFERENCES

1. Bodner, S.R. and Partom, Y., "Constitutive Equations for Elastic-Viscoplastic Strain Hardening Materials", Journal of Applied Mechanics, Transactions ASME, Vol. 42, 1975, pp. 385-389.

2. Stouffer, D.C., "A Constitutive Representation for IN100," AFWAL-TR-81-4039, 1981

3. Beaman, R.L., "The Determination of the Bodner Material Coefficients for IN718 and Their Effects on Cyclic Loading," M.S. Dissertation, Air Force Institute of Technology, Mar. 1984

4. Hinnerichs, T.D., "Viscoplastic and Creep Crack Growth Analysis by the Finite Element Method," AFWAL-TR-80-4140, 1981

5. Hinnerichs, T., Nicholas, T. and Palazotto, A.N., "A Hybrid Experimental Numerical Procedure for Determining Creep Crack Growth Rates, "Eng. Fract. Mech., Vol. 16, No. 2, 1982, pp. 265-277.

6. Sharpe, W.N. Jr., "A Technique for High Temperature Creep Displacement Measurement", Fracture Mechanics:Fourteenth Symposium - Volume II: Testing and Applications, ASTM STP 791, J.C. Lewis and G. Sines, Eds., American Society for Testing and Materials, 1983, pp. II-157-II-165.

7. Donath, R.C., Nicholas, T. and Fu, L.S., "An Experimental Investigation of Creep Crack Growth in IN100", Fracture Mechanics:Thirteenth Symposium, ASTM STP 743, Richard Roberts, Ed., American Society for Testing and Materials, 1981, pp. 186-206.

8. Smail, J. and Palazotto, A.N., "The Viscoplastic Crack Growth Behavior of a Compact Tension Specimen Using the Bodner-Partom Flow Law," Eng. Fract. Mech., Vol. 19, No. 1, 1984, pp. 137-158.

9. Keck, J.E., Nicholas, T. and Palazotto, A.N., "High Temperature Viscoplastic Fatigue Behavior of a Compact Tension Specimen," Eng. Fract. Mech. (in press).

10. Wilson, R.E., "The High Temperature Viscoplastic Fatigue Behavior of IN100 Using the Bodner-Partom Flow Law," M.S. Dissertation, Air Force Institute of Technlogy, Sept. 1983

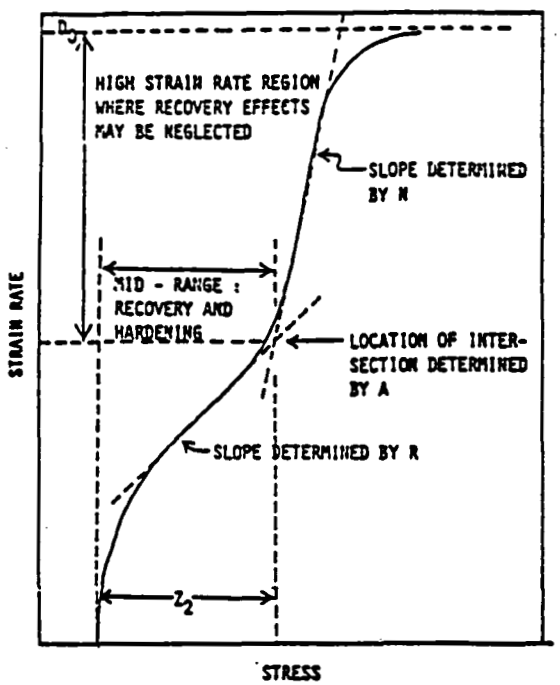

a) Overall behavior

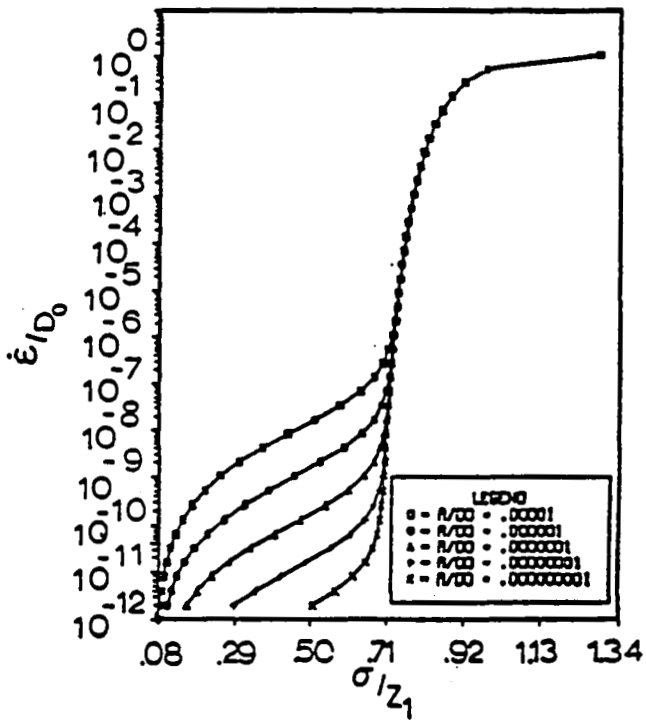

b) Variation with A.

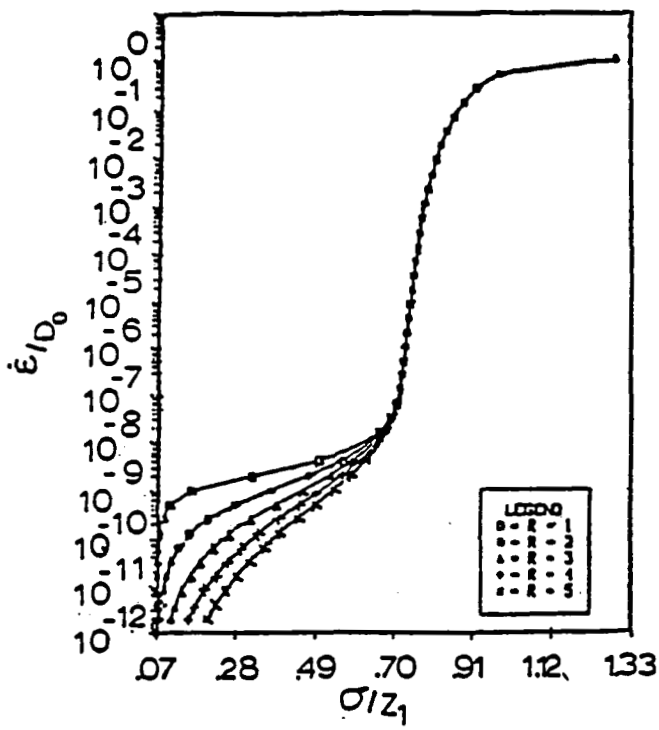

c) Variation with r.

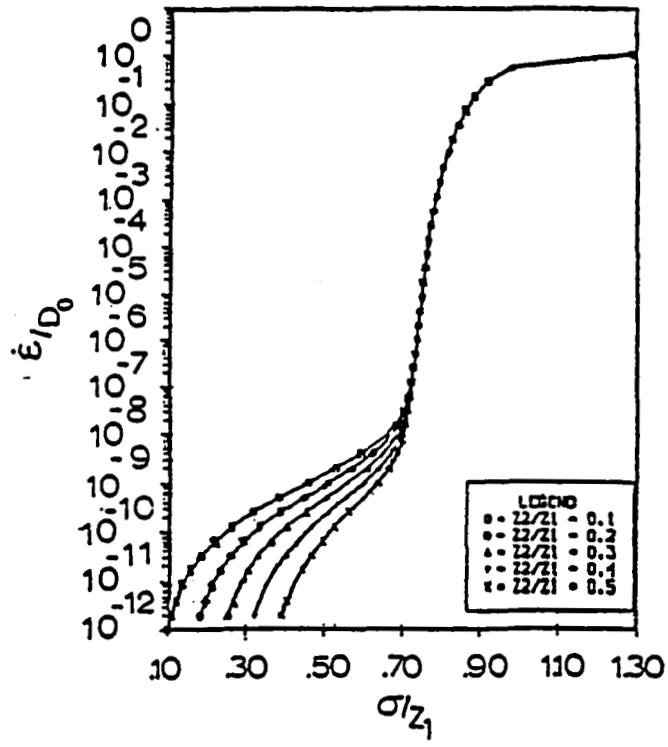

d) Variation with Z_2.

Fig. 1 Stress-strain rate response of Bodner-Partom model. (Ref. 3)

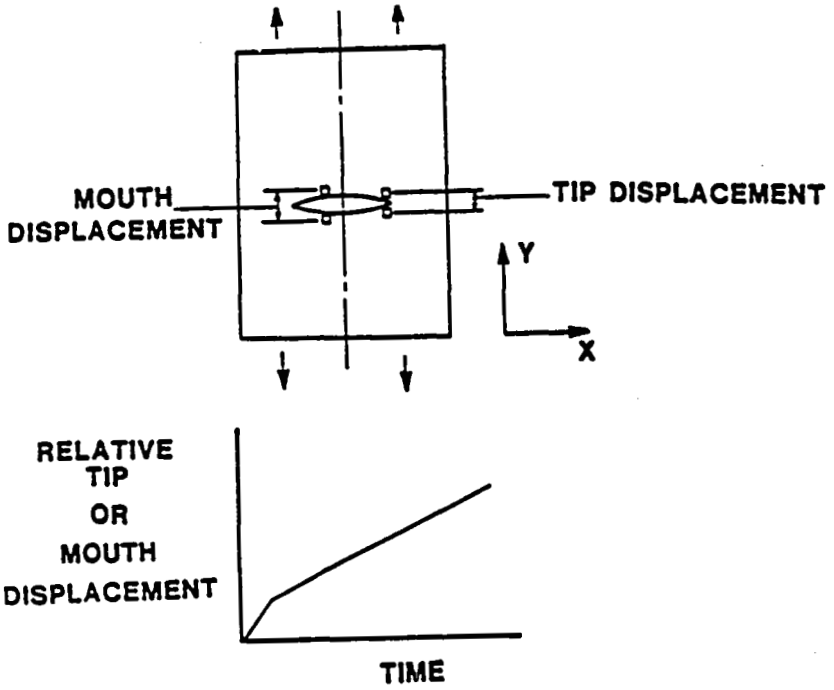

Fig. 2 Schematic of center cracked geometry showing indent locations and data.

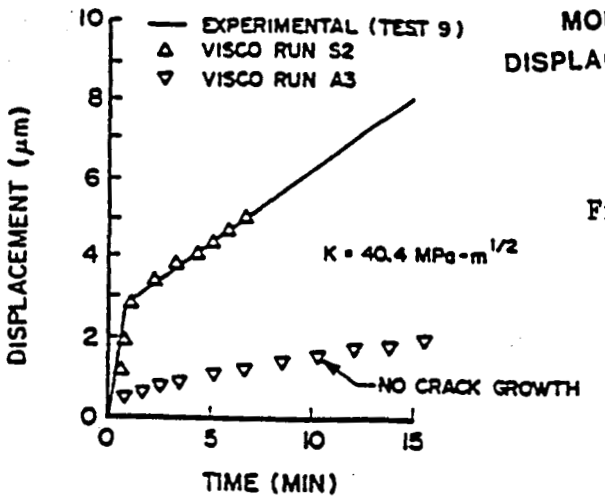

a) Displacements

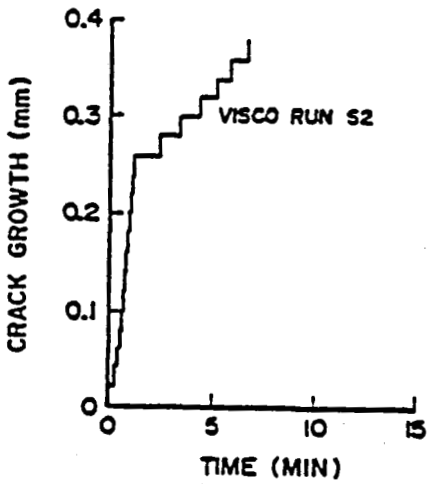

b) Crack extension

Fig. 3 Typical results from HEN procedure. (Ref. 5)

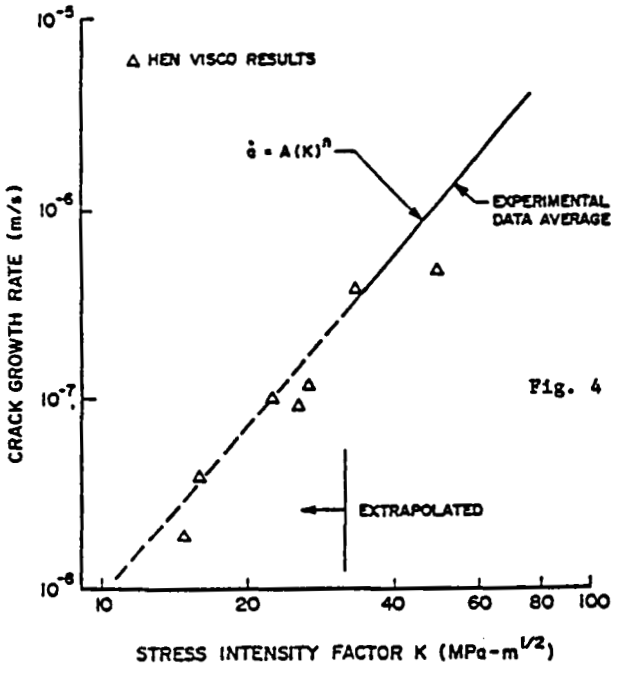

Fig. 4

Fig. 4 Sustained load crack growth rates from HEN calculations.

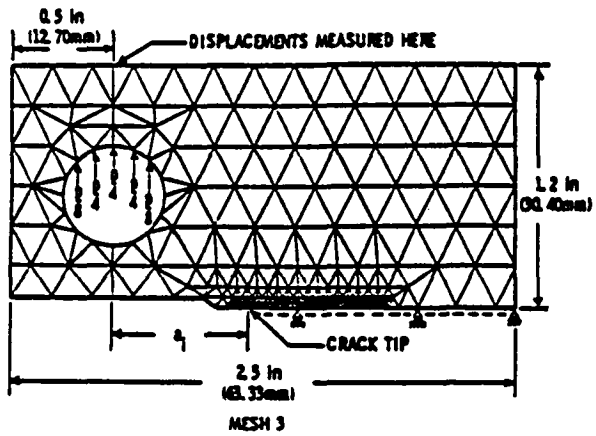

a) Finite element mesh

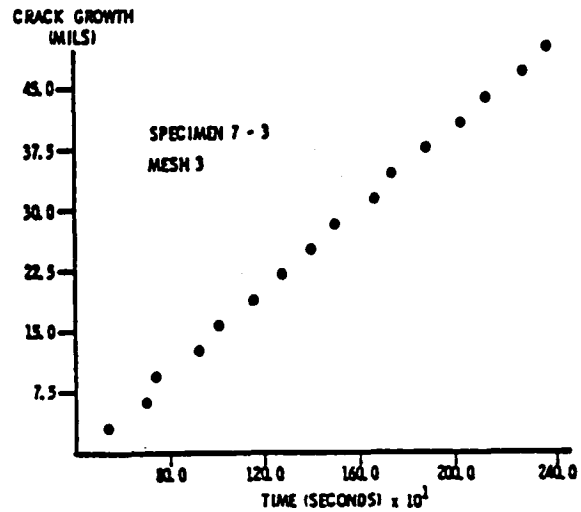

c) Computed crack extension

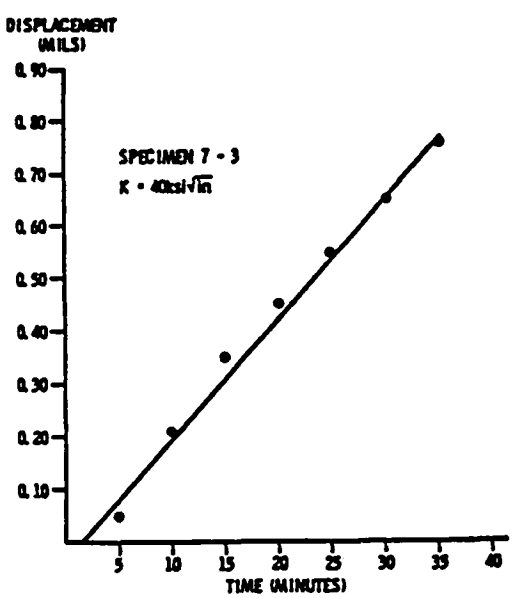

b) Computed displacements

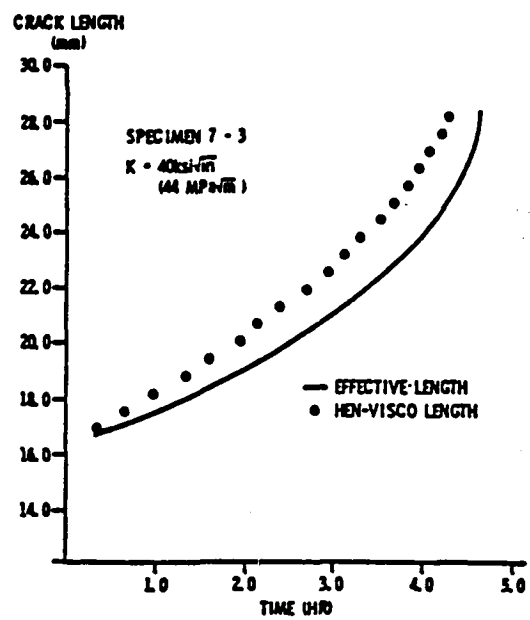

d) Comparison with experiment

Fig. 5 Typical results from application of HEN to CT geometry.(Ref. 8)

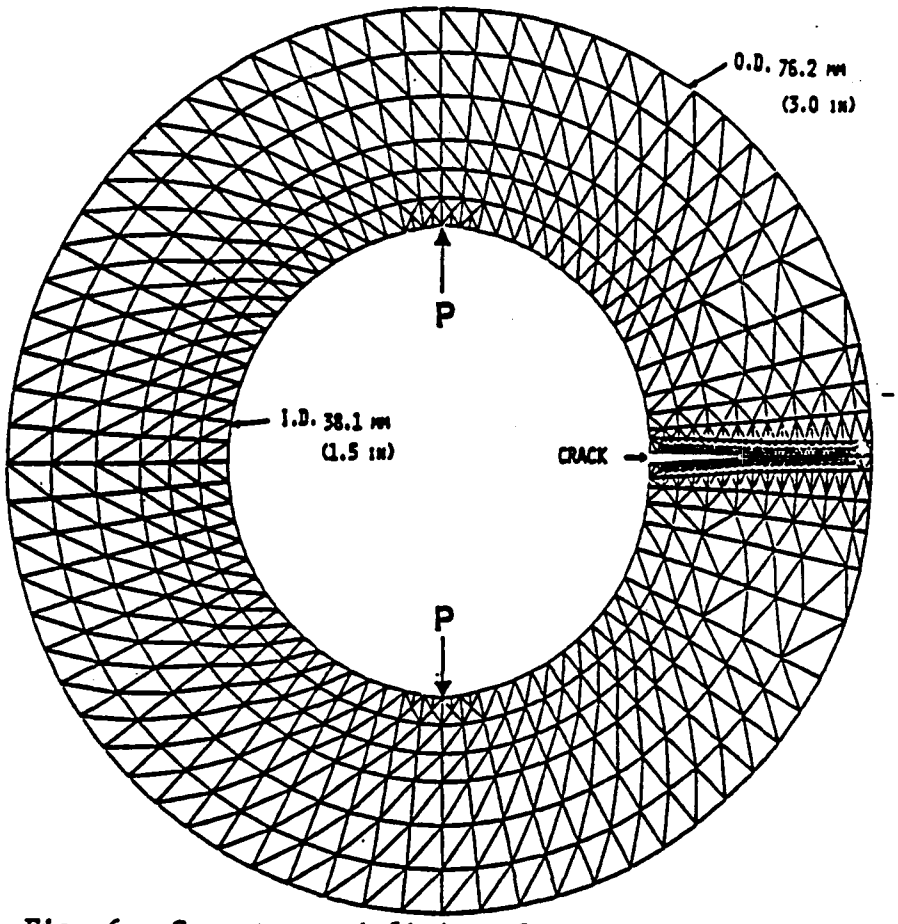

Fig. 6 Geometry and finite element mesh for cracked ring geometry.

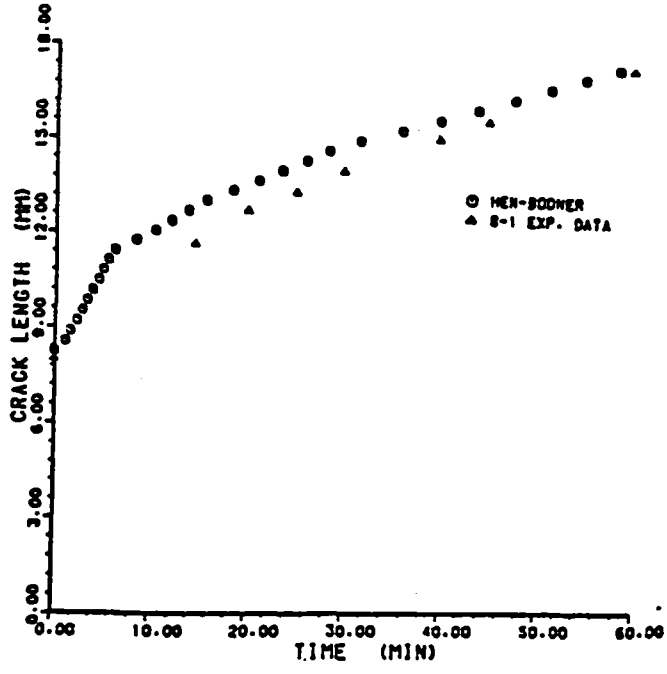

Fig. 7 Comparison of HEN crack length with experimental data for ring.

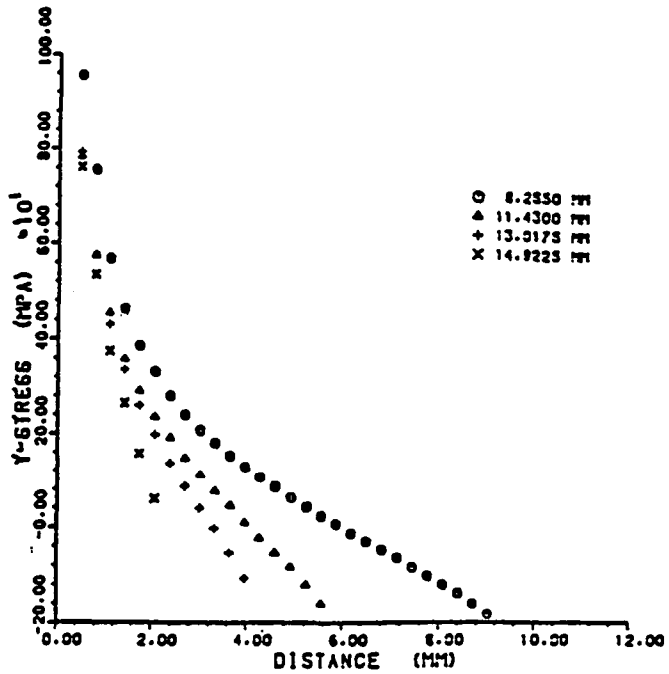

Fig. 8 Stress profile ahead of crack tip in ring.

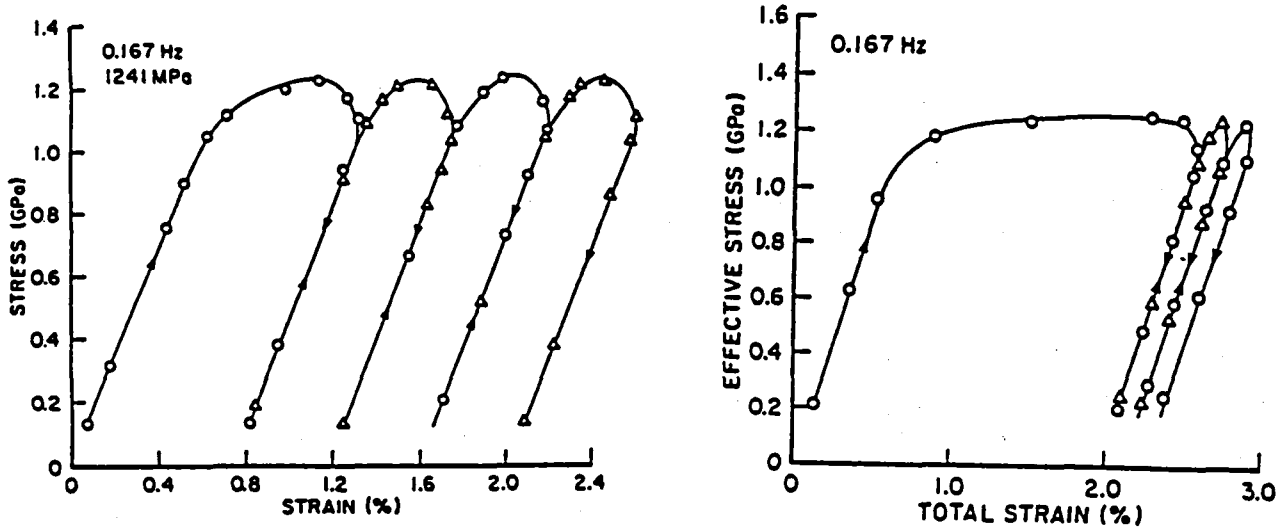

a) Uniaxial specimen

b) Ahead of crack tip in CT specimen

Fig. 9 Cyclic stress-strain response under load control at R=0.1. (Ref. 9)

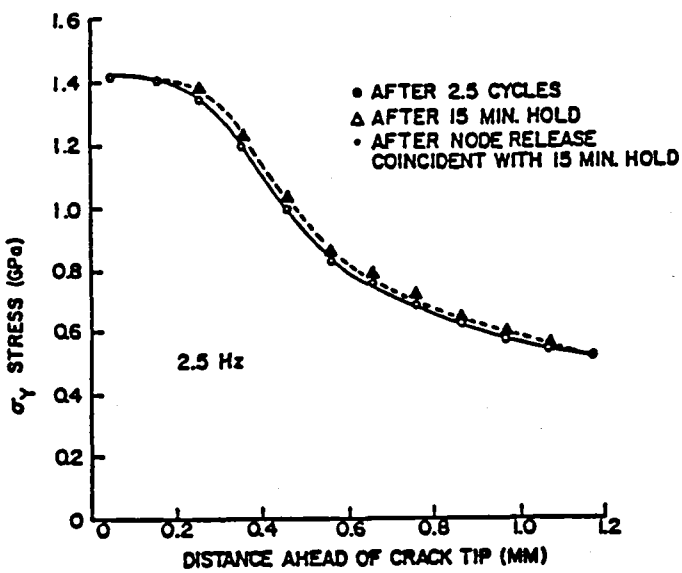

Fig. 10 Stress profiles ahead of crack tip in CT specimen, R=0.1 (Ref. 9)

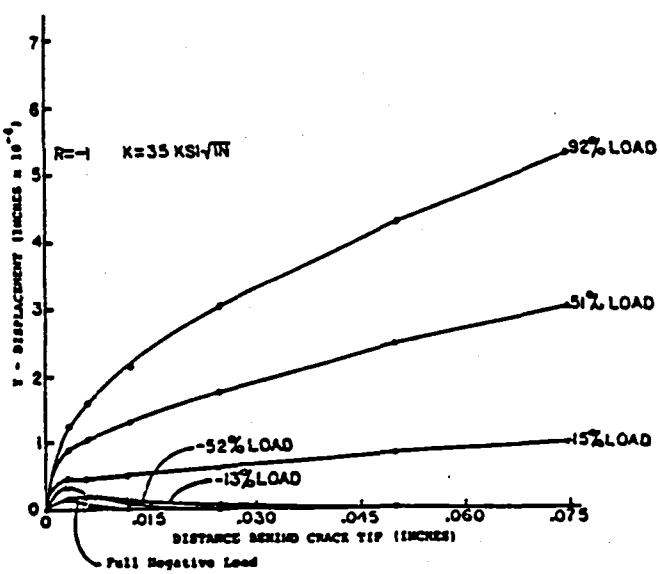

Fig. 11 Displacement profiles behind crack tip in CT specimen, R=-1 (Ref. 10)